PAPER

CrossMark
click for updates

Consideration of land use change-induced surface albedo effects in life-cycle analysis of biofuels†

H. Cai,[*a] J. Wang,[b] Y. Feng,[b] M. Wang,[a] Z. Qin[a] and J. B. Dunn[a]

Land use change (LUC)-induced surface albedo effects for expansive biofuel production need to be quantified for improved understanding of biofuel climate impacts. We addressed this emerging issue for expansive biofuel production in the United States (U.S.) and compared the albedo effects with greenhouse gas emissions highlighted by traditional life-cycle analysis of biofuels. We used improved spatial representation of albedo effects in our analysis by obtaining over 1.4 million albedo observations from the Moderate Resolution Imaging Spectroradiometer flown on NASA satellites over a thousand counties representative of six Agro-Ecological Zones (AEZs) in the U.S. We utilized high-spatial-resolution, crop-specific cropland cover data from the U.S. Department of Agriculture and paired the data with the albedo data to enable consideration of various LUC scenarios. We simulated the radiative effects of LUC-induced albedo changes for seven types of crop covers using the Monte Carlo Aerosol, Cloud and Radiation model, which employs an advanced radiative transfer mechanism coupled with spatially and temporally resolved meteorological and aerosol conditions. These simulations estimated the net radiative fluxes at the top of the atmosphere as a result of the LUC-induced albedo changes, which enabled quantification of the albedo effects on the basis of radiative forcing defined by the Intergovernmental Panel on Climate Change for CO_2 and other greenhouse gases effects. Finally, we quantified the LUC-induced albedo effects for production of ethanol from corn, miscanthus, and switchgrass in different AEZs of the U.S. Results show that the weighted national average albedo effect is a small cooling effect of -1.8 g CO_2 equivalent (CO_2e) for a mega-Joule (MJ) of corn ethanol, a relatively stronger warming effect of 12.1 g CO_2e per MJ of switchgrass ethanol, and a small warming effect of 2.7 g CO_2e per MJ of miscanthus ethanol. Significant variations in albedo-induced effects are found among different land conversions for the same biofuel, and among different AEZ regions for the same land conversion and biofuel. This spatial heterogeneity, owing to non-linear albedo dynamics and radiation processes, suggests highly variable LUC-induced albedo effects depending on geographical locations and vegetation. These findings provide new insights on potential climate effects by producing biofuels through considering biogeophysical as well as biogeochemical effects of biofuel production and use in the U.S.

Broader context

In this paper, we quantified land use change (LUC)-induced albedo effects for three major biofuels in the U.S., using a methodology that relies upon state-of-the-art satellite data products for albedo and vegetation observations and that estimates CO_2 equivalent emissions of albedo effects per IPCC's recommendations. Our analysis indicates that the LUC-induced albedo effect is small for corn and miscanthus ethanol, but is significant for switchgrass ethanol, which is driven by the types, locations, and intensities of various land conversions to these biofuel feedstocks. The albedo effects quantified in this study, which has been generally overlooked in traditional LCA, fill in an important biofuel GHG analysis gap and shed light on a fuller picture of the climate impacts of major U.S. biofuels. We aspire that this work raises awareness among policy makers and other stakeholders regarding an additional effect that can be considered when estimating biofuel life-cycle greenhouse gas emissions and offers them insight into routes to estimating equivalent GHG emissions from albedo shifts stemming from LUC associated with large-scale expansion in production of biofuels in the U.S. and challenges associated with these estimations.

[a] Systems Assessment Group, Energy Systems Division, Argonne National Laboratory, Argonne, IL, 60439, USA. E-mail: hcai@anl.gov
[b] Environmental Science Division, Argonne National Laboratory, Argonne, IL, 60439, USA
† Electronic supplementary information (ESI) available. See DOI: 10.1039/c6ee01728b

Introduction

Liquid biofuels produced from agricultural crops, dedicated energy crops, agricultural and forest residues, and other biomass feedstocks have been promoted in the U.S., the European Union,

and elsewhere, aiming towards the reduction of oil dependence and of greenhouse gas (GHG) emissions of the transportation sector. Life-cycle analysis (LCA) has been adopted as a valuable tool to evaluate GHG emissions of biofuels by regulations such as the U.S. Environmental Protection Agency's Renewable Fuel Standard (RFS),[1] California's Low Carbon Fuel Standard (LCFS),[2] and the EU Renewable Energy Directive.[3]

A focal point in the debate about the potential climate change effects of biofuels has been GHG emissions from carbon stock changes stemming from land use change (LUC) associated with biofuel feedstock production, besides GHG emissions associated with direct activities for production of biomass feedstocks and biofuels, since 2008.[4] Besides biogeochemical effects including soil organic carbon (SOC) changes, LUC also modifies the surface energy balance, moisture, latent heat fluxes, and momentum fluxes through biogeophysical mechanisms, such as surface albedo, evapotranspiration, and surface roughness.[5-14] Of these biogeophysical factors, surface albedo has been considered a dominant effect at the global scale,[15] particularly in the mid-latitude temperate and high-latitude boreal regions.[16-18] Modification of surface albedo perturbs the radiation budget by modifying the absorption of incoming solar radiation, resulting in radiative forcings that need to be considered together with the radiative forcings due to GHG emissions through biogeochemical mechanisms. However, this LUC-induced albedo effect for biomass production has received limited focus until very recently.

In particular, albedo effects associated with forest systems for bioenergy production, especially those affected by seasonal snowfall, have been studied recently.[16,19-27] Besides, albedo effects of hypothetical conversion of annual to perennial bioenergy crops[28] and conversion from cropland and pasture to sugarcane in Brazil[29] have been evaluated. The GHG emission-equivalent climate effects of both biogeochemical and biogeophysical factors including albedo effects for agricultural crops and forest systems were simulated, and biogeophysical effects were found to outperform the biogeochemical effects for agricultural ecosystems and Brazilian sugarcane systems.[30] Climate impacts of changes in surface albedo from several LUC scenarios for cultivation of biomass for bio-based diesel fuel production varied significantly and could be substantial relative to those of petroleum-derived diesel.[31] These studies suggested that LUC-induced albedo effects were potentially substantial and could even outweigh the biogeochemical effects evaluated in previous biofuel LCAs.

However, LUC-induced albedo effects of major biofuel production systems in the U.S. have yet to be examined in the context of life-cycle GHG emissions of such biofuels encouraged by RFS and LCFS. We aim to address this issue by quantifying the albedo effects of major biofuels including corn ethanol and cellulosic ethanol derived from switchgrass and miscanthus, in the U.S., and to integrate the albedo effects into life-cycle GHG intensities of these biofuels on a common basis. Corn ethanol has been produced on a mass scale in the U.S., reaching 14.8 billion gallons in 2015,[32] whereas ethanol produced from cellulosic feedstocks is being promoted in the RFS[1] and is

predicted to cause significant GHG reductions.[33] We evaluate the albedo effects associated with various LUC scenarios at the Agro-Ecological Zone (AEZ)[34] geographical level that are simulated by the Global Trade Analysis Project (GTAP) model to produce 11.6, 7.0 and 7.0 billion gallons of corn, switchgrass, and miscanthus ethanol, respectively, a year, in accordance with assumed RFS induced production levels.[35] We collected satellite measurement data for both surface albedo and surface land covers at high spatial resolution, covering most of the regions in the U.S. where corn, switchgrass, and miscanthus are grown or could be grown for ethanol production. The analysis on the AEZ level assures a consistent spatial resolution with our analysis of soil organic carbon (SOC) changes (biogeochemical effects) associated with the production of these biofuels,[36,37] and thus enables the comparison and integration of albedo effects with SOC change effects resulting from the same LUC scenarios for these biofuel production systems in the U.S.

The quantified albedo effects in this analysis shed light on the key question of whether these biofuels still offer overall climate change benefits, and if so, the magnitude of the benefits, compared to petroleum fuels.

Methodology and data

We started our analysis with defining LUC scenarios associated with biofuel production. Then, we retrieved albedo and land cover satellite observations and paired them on a geospatially consistent basis. We next analysed the albedo dynamics associated with specific land covers, and used them to drive a cloud and aerosol coupled radiation model to simulate the radiative forcings due to LUC-induced changes in albedo. Finally, we adopted a radiative forcing-based metric[18,19,23,38,39] to evaluate LUC-induced albedo effects. LUC-induced surface albedo changes perturb the radiation budget by modifying the absorption of incoming solar radiation, resulting in radiative forcings that are similar to the radiative forcings due to GHG emissions. This approach allows for quantification of albedo effects to equivalent CO_2 emissions, which can be integrated with GHG emissions associated with the life cycle of biofuels.

Fig. S1 (ESI†) presents a flowchart depicting our methodology quantifying LUC-induced albedo effects of biofuel production in the U.S. The details of this methodology are given below.

Land use change scenarios associated with biofuel production

Tables 1–3 report the GTAP LUC scenarios and the acreage of individual LUCs at the AEZ level that we considered for corn, switchgrass, and miscanthus ethanol, respectively.[35] We considered land cover types including cornfields, switchgrass fields, miscanthus fields, grassland, cropland/pasture land, shrubland, and forest. For corn ethanol, conversions from cropland/pasture land and from grassland to cornfields are the dominant LUC types, while cropland/pasture land is the predominant land type to be used for switchgrass or miscanthus production as ethanol feedstocks. In this study, we focused on AEZ 7, AEZ 8, AEZ 9, AEZ 10, AEZ 11, and AEZ 12 in the U.S., where corn and energy

Table 1 Land use change at the U.S. AEZ level, in hectares[a], for corn ethanol production of 11.6 billion gallons a year according to 2011 GTAP simulations[35]

From	Forest	Grassland	Cropland/Pasture land	Shrubland
To	Cornfields	Cornfields	Cornfields	Cornfields
AEZ 7	4436	340 320	224 128	−957
AEZ 8	7269	133 912	102 281	9662
AEZ 9	2066	10 238	64 792	−44
AEZ 10	132 412	82 626	403 376	47 224
AEZ 11	92 924	42 881	298 278	436
AEZ 12	23 532	14 111	74 470	6532
AEZ 13	273	11 662	1340	463
AEZ 14	1912	3518	278	3120
AEZ 15	73	214	0	127
AEZ 16	1	3	0	4

[a] Positive numbers represent the number of hectares of original land cover that is converted to cornfields. Negative numbers represent reverse conversions.

grasses are mostly or likely to be grown. We didn't consider LUCs occurring in AEZ 13, AEZ 14, AEZ 15, or AEZ 16, as these are not primary agricultural regions in the U.S. Fig. S2 (ESI†) shows a map of the AEZs over the contiguous U.S. (CONUS). We assumed that these LUC scenarios would last for 30 years for our albedo analysis, the time horizon assumed by the

U.S. EPA and California Air Resources Board in ethanol LUC evaluations.

Moderate resolution imaging spectroradiometer (MODIS) albedo data

Satellite data provide a unique opportunity for quantifying surface albedo on a global basis. We used MCD43A3 Version 5 albedo data products generated by Moderate Resolution Imaging Spectroradiometer (MODIS) on board the Terra and Aqua satellites.[40] These products have been validated extensively and have been widely used as a benchmark for evaluating other satellite albedo products.[41–45] A complete set of quality control flags is contained in MCD43A2, which accompanies the MCD43A3 data product and describes the quality of the albedo observations. In this analysis, we retrieved albedo data with excellent and good data quality ratings that exhibit minimal uncertainty. In this analysis, we used black-sky albedo (BSA), which is defined as albedo in the absence of a diffuse component, as a proximate to actual albedo, or the so-called blue-sky albedo, which is a mix of BSA and white-sky albedo (WSA) that is defined as albedo in the absence of a direct component when the diffuse component is isotropic. It is known that BSA is dependent on solar zenith angle, while WSA is not.[46] The impact on the results with use of the BSA is probably small as BSA and WSA

Table 2 Land use change at the U.S. AEZ level, in hectares[a], for switchgrass ethanol production of 7 billion gallons a year according to 2011 GTAP simulations[35]

From	Forest	Forest	Grassland	SWG fields	Cropland/Pasture land	SWG fields	Shrubland	Shrubland
To	SWG[b] fields	Grassland	SWG fields	Grassland	SWG fields	Cropland/Pasture land	SWG fields	Grassland
AEZ 7	63 362	0	16 432	0	2 818 337	0	−13 674	0
AEZ 8	0	34 289	0	1374	1 001 533	0	0	45 580
AEZ 9	824	32 787	0	0	340 944	0	−17	−693
AEZ 10	70 444	102 054	0	0	1 675 529	0	25 124	36 397
AEZ 11	84 058	100 194	0	0	1 737 505	0	394	470
AEZ 12	32 176	58 568	0	0	754 337	0	8931	16 256
AEZ 13	2752	16 640	0	0	0	39 839	4654	28 146
AEZ 14	2479	9430	0	0	0	10 468	4046	15 395
AEZ 15	83	666	0	0	0	0	145	1167
AEZ 16	1	5	0	0	0	0	6	26

[a] Positive numbers represent the number of hectares of original land cover that is converted to switchgrass, grassland, or cropland/pasture land. Negative numbers represent reverse conversions. [b] Switchgrass.

Table 3 Land use change at the U.S. AEZ level, in hectares[a], for miscanthus ethanol production of 7 billion gallons a year according to 2011 GTAP simulations[35]

From	Forest	Forest	Grassland	Cropland/Pasture land	Miscanthus fields	Shrubland	Shrubland
To	Miscanthus fields	Grassland	Miscanthus fields	Miscanthus fields	Cropland/Pasture land	Miscanthus fields	Grassland
AEZ 7	15 706	0	17 600	1 486 004	0	−3390	0
AEZ 8	2470	6168	0	638 835	0	3284	8200
AEZ 9	821	7512	0	230 913	0	−17	−159
AEZ 10	28 414	21 443	0	1 061 039	0	10 134	7647
AEZ 11	35 669	20 482	0	911 373	0	167	96
AEZ 12	14 253	13 225	0	275 172	0	3956	3671
AEZ 13	890	3868	0	0	10 809	1505	6543
AEZ 14	724	2229	0	0	2795	1182	3638
AEZ 15	28	158	0	0	0	49	277
AEZ 16	0	1	0	0	0	2	6

[a] Positive numbers represent the number of hectares of original land cover that is converted to miscanthus, grassland, or cropland/pasture land. Negative numbers represent reverse conversions.

from MODIS are close to each other.[43] Fig. S3 (ESI†) shows more than 5.7 million BSA and WSA observations, respectively, at a resolution of 500 meter by 500 meter in one tile of albedo data covering part of the U.S. Midwest, as an example.

To reduce the temporal variability of albedo associated with inter-annual variability in phenology and local climate, we used eight-day MODIS albedo data in 2014, which was a climatically neutral year that may represent a long-term climatological mean of climatic parameters well. For example, the annual average precipitation in 2014 was about ±20% of the 30 year average over much of CONUS. Also, 2014 was neither an El Niño nor a La Niña year, which could otherwise have a significant impact on the climatic conditions over CONUS, affecting the vegetation growth conditions and thus their albedo effects.

Land cover data

Land cover data that can be paired with MODIS albedo data are needed for recognition of specific land cover types the albedo data represent. The MODIS land cover data product, MCD12Q1, has the same spatial resolution as MCD43A3 and is thus suitable to pair with the albedo data for a given land cover type. However, MCD12Q1 adopts International Geosphere Biosphere Programme, which aggregates cropland and natural vegetation as a generalized land cover type.[47] To identify specific cropland types, such as agricultural land producing corn or soybeans, we used a geospatial land cover data product called the Cropland Data Layer (CDL).[48] CDL data have covered the entire CONUS since 2008. The CDL is a raster, geo-referenced, crop-specific land cover dataset in the Albers Equal-Area Conic geographic projection and in GeoTIFF format, which is created annually by the U.S. Department of Agriculture (USDA) for the CONUS. CDL contains more than 100 (depending on year) land cover types, including cropland types (e.g., corn, soybean, and sorghum), wetland, forest, and vegetables/fruits (e.g., apple). The latest CDL data have a ground resolution of 30 by 30 meters. Fig. S4 (ESI†) shows about one million parcels of fields (pixels) at the high spatial resolution for corn and soybean in Adair County, Iowa, in 2014, as an example.

Geographical pairing of MODIS albedo data and CDL land cover data

We paired MODIS albedo data and CDL land cover data on a consistent geospatial basis to identify the albedo dynamics associated with a specific land cover. We managed to identify and retrieve ''clean pixels'' that represent ''clear-cut areas'' of a specific type of land cover at an approximate 500 meter resolution by overcoming three challenges for data processing. A detailed explanation of the challenges and a pairing method developed to address them is provided in the associated ESI,† Section S1. It is noted that we applied a 100% threshold for this spatial pairing, which ensures that each albedo observation retrieved represented exclusively a specific type of land cover. Fig. S5 (ESI†) provides an example of applying the geographical pairing technique to identify cornfields with varying minimum thresholds of corn area coverage percentages within 500 meter pixels in Delaware County, Iowa.

Retrieval of land-cover-specific albedo data

Albedo is dependent on the solar zenith angle and the type, density, and spectral properties of land covers.[49] It is site-specific even for the same type of land cover.[30] To include albedo effects associated with spatial variability in phenology of crops and local climate, we retrieved albedo data from multiple locations within each AEZ for each land cover type considered in this study.

For corn, we chose multiple counties within each AEZ where the county-level corn production is among the top 30% of all counties,[37,48] of which the corn production accounted for about 71% of the total U.S. corn production in 2014.[50] For switchgrass, miscanthus, cropland, grassland, forest, and shrubland, we chose the top 20% counties by growth area within each AEZ according to county-level summary statistics on the land cover acreages.[48] For cropland, we first identified the most abundant crop type within each AEZ according to CDL county-level summary statistics on the cropland acreage by type;[48] we then selected the top 20% counties by area for the major crop type in each AEZ. For forest, the dominant type of forest varies regionally, and can be either deciduous forest or evergreen forest, both of which we considered.

The CDL data do not classify miscanthus as a specific type of land cover, since there is no commercial growth of miscanthus in the U.S., and switchgrass acreage in the database is very limited. We assumed that the surface albedos of both switchgrass and miscanthus resemble those of grassland, as they are both herbaceous perennial grasses. We also assumed that pasture land has a similar surface albedo to grassland, and used grassland albedo observations as surrogates for those of pasture land, because of the lack of pasture-specific land cover classification. We assumed that the land use category of cropland/pasture land consists of 50% cropland and 50% pasture. Furthermore, soybean or winter wheat, which is the dominant type of cropland in the AEZs of interest, was used to represent cropland that is converted for cornfields for ethanol production, while the cropland converted for switchgrass and miscanthus growth was assumed to consist of 50% cornfields, and 50% soybean fields or 50% winter wheat fields.

We applied the geographical pairing technique to retrieve all the 500 meter-resolution albedo observations over identified clean pixels of the land cover of interest in these selected counties. Fig. S6 (ESI†) shows the county-level BSA retrieved for corn and forest as an example. We retrieved BSA and their data quality flags from those identified clean pixels from 10 tiles of the MCD43A3 and MCD43A2 datasets, to cover much of each AEZ. We employed Mira, a supercomputing system at Argonne National Laboratory,[51] to meet the demanding computing requirements for pairing and retrieving albedo data over a variety of land cover types in dozens of counties within each AEZ, as shown in Table S1 (ESI†). Fig. 1 shows the geographical distributions of the counties with retrieved clean-pixel albedo data for each land cover type within each AEZ. With the large

2858 | *Energy Environ. Sci.*, 2016, **9**, 2855–2867

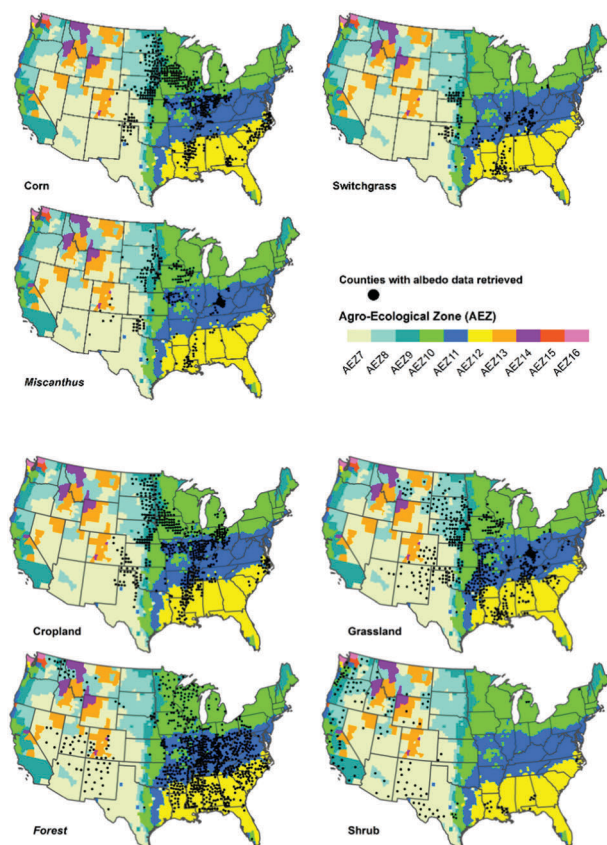This journal is © The Royal Society of Chemistry 2016

Fig. 1 Geographical distribution of counties with clean-pixel albedo observations retrieved for cornfields, switchgrass fields, miscanthus fields, cropland, forest, grassland, and shrubland in AEZ 7 to AEZ 12. Cropland is represented by winter wheat in AEZ 7 and soybean in other AEZs, as these are the most prevalent crop types in those AEZs, according to the cropland data layer.[48]

number of clean-pixel albedo observations retrieved from various locations for most land cover types within each AEZ, we greatly improved the spatial representation of the albedo observations for specific land cover types at the AEZ level, allowing investigation of spatial variation in the LUC-induced albedo effect associated with biofuel production.

Radiative-forcing modelling of albedo changes

Radiative forcing, or the perturbation to the global radiation budget prior to any feedback resulting from the response of other aspects of the climate system,[28] is a metric that can be used to compare the effects of changes in surface albedo with the effects of changes in GHG emissions. Radiative forcing from albedo changes can be integrated within the LCA framework for comparing with radiative forcings from GHG emissions, but high spatial and temporal resolution for radiative forcing modelling is required.[52]

We used the Monte Carlo Aerosol, Cloud and Radiation (MACR) model[53,54] to simulate the shortwave radiative forcing due to surface albedo changes over a specific type of land cover. The model was developed on the basis of the so-called Monte Carlo Independent Column Approximation approach,[55] and

simulated radiative fluxes, in W m^{-2}, at the top of the atmosphere (TOA). The ESI,† Section S2 has details on the physical parameterization and validation of the model.

The Monte Carlo approach for solving the radiative transfer equation is advantageous over two-stream approximations, e.g.,[56] as it calculates the atmospheric fluxes more accurately than can be done with for both clear and cloudy skies. In this study, MACR used an advanced radiative transfer coupled with spatially and temporally resolved meteorological and aerosol conditions. In the estimation of perturbations in global energy balance due to changes in land surface albedo, it is advantageous over previous studies that used an atmospheric transmittance factor, directly adopted estimates of the incoming solar radiation flux at surface level, or relied on simple empirical calculations.[31,52] For instance, Cherubini et al. adopted a constant of 0.854 denoting the globally averaged annual fraction of upwelling shortwave radiation exiting a clear sky.[52] The use of such a constant transmittance does not take into account spectral variations in absorption or reflection as well as its dependence on zenith angle.

MACR takes eight-day albedo data as one of the key inputs in simulating the resulting radiative fluxes at the TOA. The ESI,† Section S2 presents details on data for input parameters and methodology for radiation simulations performed by the model. Fig. S7 (ESI†) shows temporal variation in net radiation at the TOA over cornfields in AEZ 7 in 2014, as an example. Table S2 (ESI†) summarizes annual average diurnal net radiative flux for each land cover type within each AEZ predicted by MACR.

Calculation of CO_2 equivalent emissions of albedo effects

We adopted the Global Warming Potential (GWP) metric on a 100 year time horizon according to the IPCC Fifth Assessment Report methodology[57] for direct comparison of albedo-induced radiative forcing with the radiative forcing effects of GHG emissions. Net radiative fluxes simulated by MACR for specific land covers were used to calculate the radiative forcings and further the GWP associated with various LUC scenarios. This allows for translation of LUC-induced albedo effects to CO_2 equivalent (CO_2e) emissions on per square meter of LUC basis. This approach was applied to LUC by LUC at the AEZ level, and the AEZ-level CO_2e emissions for LUC-induced albedo effects were aggregated on the basis of the types and magnitudes in acreage of the LUC scenarios to represent the total albedo effects for production of 11.6, 7.0, and 7.0 billion gallons of corn, switchgrass, and miscanthus ethanol annually. In the end, we calculated CO_2e emissions for the LUC-induced albedo effects associated with corn, switchgrass, and miscanthus ethanol on per mega-Joule (MJ) of ethanol basis for these biofuels. The ESI,† Section S3 presents details on the methodology of calculation of CO_2e emissions for LUC-induced albedo effects.

Results and discussion

In this section, we first present results for land cover-specific albedo dynamics and the resultant net radiative fluxes. These results lead to the subsequent investigation of the direction,

This journal is © The Royal Society of Chemistry 2016

Energy Environ. Sci., 2016, 9, 2855–2867 | 2859

magnitude, and drivers of the LUC-induced albedo effects associated with production of corn, switchgrass, and miscanthus ethanol in the U.S.

Land cover-specific albedo dynamics

To explore the albedo effects, we retrieved 1 444 871 eight-day MODIS albedo observations from 3014 county/land cover combinations in the U.S. in 2014, and paired them geographically with land cover-specific CDL data at a spacing of 500 by 500 meters. This approach leads to an evaluation of land cover-specific albedo dynamics at an eight-day interval throughout year 2014. Fig. 2 shows the temporal variation in the eight-day BSA for cornfields, switchgrass fields, miscanthus fields, cropland/pasture land (for conversion to cornfields), cropland/pasture land (for conversion to switchgrass and miscanthus fields), forest, grassland, and shrubland in zones AEZ 7 through AEZ 12. Retrieval and analysis of albedo dynamics in multiple locations provide the opportunity to explore the albedo effects associated with a LUC that occurs in various areas within each AEZ and in various AEZs.

Fig. 2 shows that the BSA varies among different land covers within the same AEZ throughout the year, particularly in the off-season (October to March), which indicates a likely impact from snow events that increase the BSA significantly during the off-season as compared to the growing season (April to September). Besides, the albedo of the same land cover can vary significantly from one AEZ to another, showing a clear region-specific characteristic of albedo dynamics even for the same type of land cover.

Forest is shown to have the lowest albedo among the land covers during most of the year in AEZs 7, 8, and 9. However, shrubland has the lowest albedo during most of the year in AEZs 10 and 11, with a value about 0.03–0.06 lower than the shrubland albedo in AEZs 7, 8, and 9. Forest and shrubland exhibit the lowest albedo in AEZ 12. This result indicates the albedo effect of heterogeneous shrubland and forest cover conditions, e.g., the varying heights and densities of the vegetation in various regions. Forest in AEZs 7, 8, and 9 has lower albedo than forest in AEZs 10, 11, and 12, as shown in Fig. 2. This is a reflection of the dominance of evergreen forest in the forest systems in the western U.S. (AEZs 7, 8, and 9), and the dominance of deciduous forest in the forest systems in the eastern U.S. (AEZs 10, 11, and 12).[48] The albedo of all land cover types exhibits a relatively smaller extent of fluctuation throughout the year in AEZ 12, as compared to the albedo dynamics in other AEZs. This result is mostly due to a difference in snowfall frequency among different AEZs. The warmer climate in AEZ 12
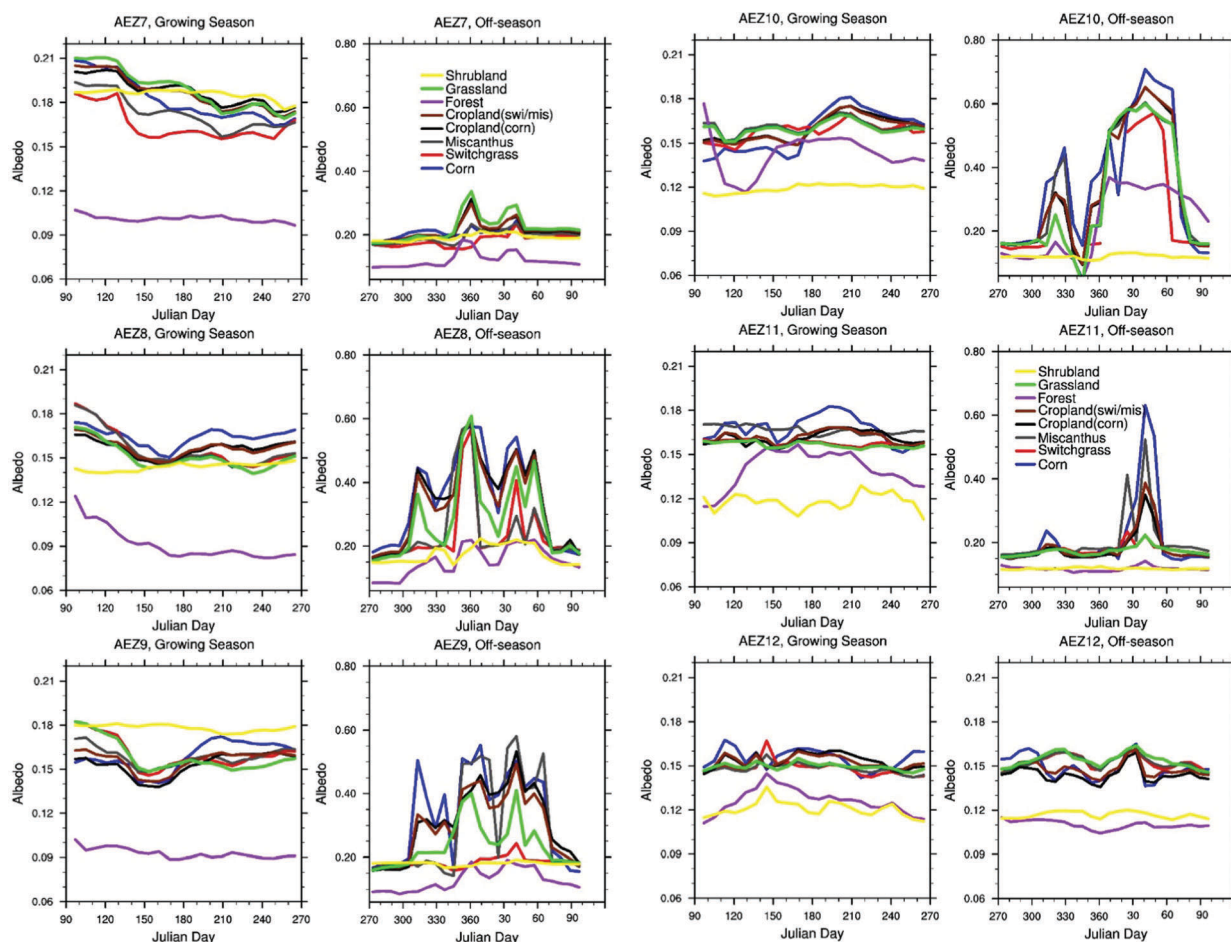

Fig. 2 Temporal variation in eight-day BSA weighted by the number of selected clean pixels of various land covers in AEZs 7–12 in the U.S. in 2014.

in the southeastern U.S., which has little snowfall, contributes to a relatively small annual variation in the albedo there.

Tables S3–S9 (ESI†) summarize the pixel count-weighted average albedo and the weighted standard deviation of albedo for the eight-day periods by AEZ and by land cover type.

Net radiative fluxes associated with land cover-specific albedo dynamics

The MACR-based simulations of the radiative fluxes at the TOA vary in response to the land cover-specific albedo dynamics, which vary from location to location even for the same type of land cover because of spatial variation in incoming solar radiation intensity, albedo dynamics, and local climate conditions. Fig. 3 shows the temporal variation in eight-day average net radiative forcings at the TOA for cornfields, switchgrass fields, miscanthus fields, cropland/pasture land (for conversion to cornfields), cropland/pasture land (for conversion to switchgrass and miscanthus fields), forest, grassland, and shrubland in AEZ 7 to AEZ 12.

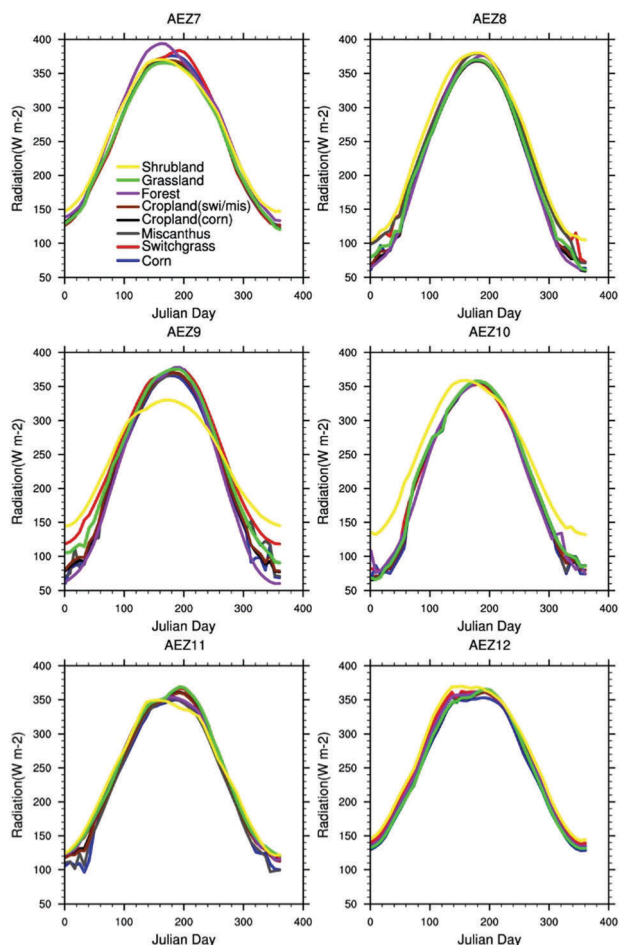Fig. 3 shows that for all land cover types in all AEZs, the eight-day average net radiation at the TOA increases from the beginning of the year, when the incoming radiation is not strong and the albedo is usually high, and reaches the peak at around the middle of the year, when the incoming radiation is strong and the albedo is typically low. Besides, the difference in the net radiation at the TOA among land covers can vary from as much as >60 W m^{-2} in some winter periods to as much as >50 W m^{-2} in some summer periods. However, this difference depends on the types of land covers and the region. The temporal variation patterns of the average net radiation at the TOA for all land covers are much smoother than the albedo variation patterns because in addition to albedo, the temporal variation patterns of other climatic factors, such as incoming solar radiation intensities, and other environmental factors, such as aerosol and ozone, could be affecting factors in the temporal variation patterns of the average net radiation at the TOA.

Tables S10–S18 (ESI†) summarize the pixel count-weighted average radiative fluxes and the weighted standard deviation of radiative fluxes for the eight-day periods by AEZ and by land cover type.

LUC-specific albedo effects for production of corn, switchgrass, and miscanthus ethanol

We calculated the CO_2e emission factors for LUC-induced albedo effects in each AEZ for corn (Fig. 4), miscanthus (Fig. S8, ESI†), and switchgrass ethanol (Fig. S9, ESI†), respectively.

With Fig. 4 for corn ethanol as an example, the albedo effects of LUCs associated with corn ethanol production vary significantly within the same AEZ for the same land conversion, as indicated by the large error bars that represent the upper, or the 97.5 percentile, and lower bounds, or the 2.5 percentile, of the albedo effects in Fig. 4. Forest conversions to cornfields exhibit a cooling climate effect in AEZs 7, 11, and 12, where the cooling effect translates to an equivalent CO_2 sequestration of as much as about 298 g CO_2e per m^2, on an area-weighted average (all numerical results hereafter are area-weighted averages, unless otherwise stated), in AEZ 11. This LUC, however, could
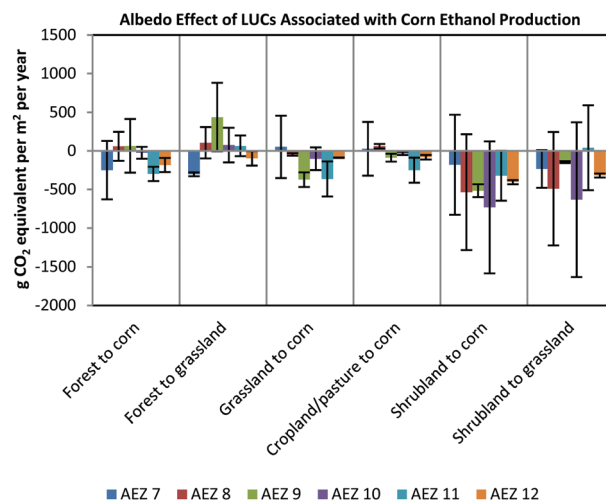
Fig. 3 Temporal variation in the eight-day average net radiation at the TOA weighted by the number of selected clean pixels of various land covers in AEZs 7–12 in the U.S. in 2014, as simulated by the MACR model.

Fig. 4 Albedo effects at the AEZ level, in g CO_2e per m^2 per year, of different LUC types associated with corn ethanol expansion scenarios.

This journal is © The Royal Society of Chemistry 2016

Energy Environ. Sci., 2016, **9**, 2855–2867 | **2861**

result in a warming climate effect of about 60–66 g CO_2e per m^2 in AEZs 8 and 9. The large variation in the albedo effect stems from wide spatial variations in albedo over both the forests and cornfields within the AEZ region, as shown in Fig. 4. For a land conversion that converts forest to grassland, the resultant albedo effect can vary from a cooling effect of about −302 g CO_2e per m^2 in AEZ 7 to a warming effect of about 438 g CO_2e per m^2 in AEZ 9. Conversion from grassland to cornfields generally induces a cooling effect in all AEZs except in AEZ 7, where an average warming effect would persist. The greatest cooling effect would occur in AEZ 9, with an equivalent carbon sequestration of about −372 g CO_2e per m^2. A conversion of 50% of cropland, represented by either soybean fields in AEZs 7–11 or winter wheat fields in AEZ 12, and 50% of pasture land represented by grassland converted to cornfields would result in a warming effect of about 28 and 62 g CO_2e per m^2, on average, in AEZs 7 and 8, respectively, but a cooling effect of as much as −250 g CO_2e per m^2, on average, in AEZ 11 and a relatively smaller cooling effect in other AEZs. Conversion from shrubland to cornfields would exert a significant cooling effect in all AEZs, ranging from −179 g CO_2e per m^2 in AEZ 7 to −731 g CO_2e per m^2 in AEZ 10. Conversion from shrubland to grassland would also exert a significant cooling effect of as much as −631 g CO_2e per m^2 in AEZ 10 and a relatively smaller cooling effect in other AEZs, except in AEZ 11, where a warming effect of 42 g CO_2e per m^2 would be expected. This cooling effect is consistent with a counter warming effect for a shift from grassland to shrubland because of dark areas created by shrubland that allows extra sunlight to be absorbed.[58] Therefore, the albedo effect is highly location-specific and land-cover-specific and varies significantly among various land covers within the same AEZs and among AEZs for the same land cover. We observed similar characteristics of the LUC-induced albedo effects associated with switchgrass and miscanthus ethanol (see ESI,† Fig. S8 and S9).

Aggregated albedo effects of production of corn, switchgrass, and miscanthus ethanol

We combined the areas of different land conversions associated with production of corn ethanol as simulated with GTAP (in Tables 1–3) with LUC type-specific albedo changes (Fig. 4 and Fig. S8, S9, ESI†) to generate results for the three ethanol types. Fig. 5 presents results for corn ethanol, Fig. S10 for switchgrass ethanol, and Fig. S11 for miscanthus ethanol, ESI.†

For corn ethanol in Fig. 5, the aggregated albedo effect for corn ethanol shows clear cooling effects in AEZs 10 and 11. Cooling effects range from −0.046 teragrams (Tg) CO_2e in AEZ 8 to −1.2 Tg CO_2e in AEZ 11, except in AEZ 7, where a warming effect of 0.24 Tg CO_2e, on average, was estimated to be emitted, mostly owing to conversion from grassland to cornfields. In AEZ 11, where the most significant cooling albedo effect was noted, a conversion from cropland/pasture land to cornfields is the dominant cause, contributing to an equivalent sequestration of 0.75 Tg CO_2e, on average, followed by an equivalent sequestration of 0.28 and 0.16 Tg CO_2e for conversion from forest and grassland to cornfields, respectively. Conversion from shrubland to cornfields in AEZ 10 leads to a cooling effect
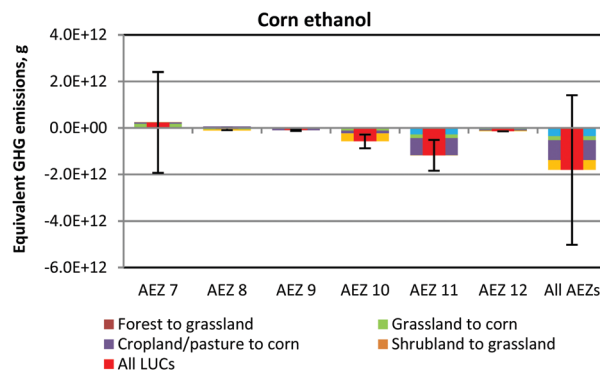

Fig. 5 Aggregated LUC-induced albedo effects at the AEZ level for corn ethanol production.

of −0.35 Tg CO_2e, followed by −0.12, −0.083, and −0.031 Tg CO_2e for a conversion from cropland/pasture land, grassland, and forest to cornfields, respectively, in the region. The overall albedo effects in AEZs 8, 9, and 12 are relatively small, owing to offsetting albedo effects of different land conversions occurring in AEZs 8 and 9, and to a small land-conversion-specific albedo effect for conversion from cropland/pasture land to cornfields in AEZ 12, the dominant conversion there (see Table 1), as shown in Fig. 5. The total albedo effect from all the land conversions occurring in all AEZs results in a net cooling effect of −1.8 Tg CO_2e, with all of the four types of land conversions associated with corn ethanol production contributing to a net cooling effect. Driven mostly by the very large variations in the land conversion-specific albedo effects in AEZ 7, particularly for conversion from cropland/pasture land to cornfields, which is the dominant type of LUC (accounting for 55% of all converted areas) in AEZ 7, the overall variation in the albedo effect for corn ethanol can vary from a cooling effect of as much as −5.0 Tg CO_2e to a warming effect of 1.4 Tg CO_2e.

For switchgrass ethanol (Fig. 6), a warming albedo effect, on average, is estimated in all the AEZs, ranging from 0.23 Tg CO_2e in AEZ 7 to 2.09 Tg CO_2e in AEZ 11, mostly owing to a shift from cropland/pasture land to switchgrass fields. Combining all AEZs leads to a total warming effect of 6.82 Tg CO_2e, on average, for switchgrass ethanol. Note that the warming effect of the conversion
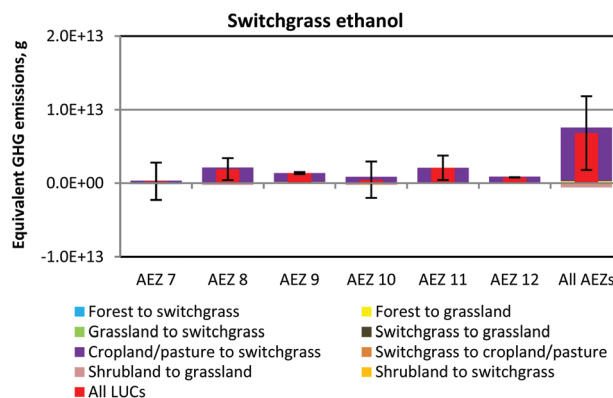

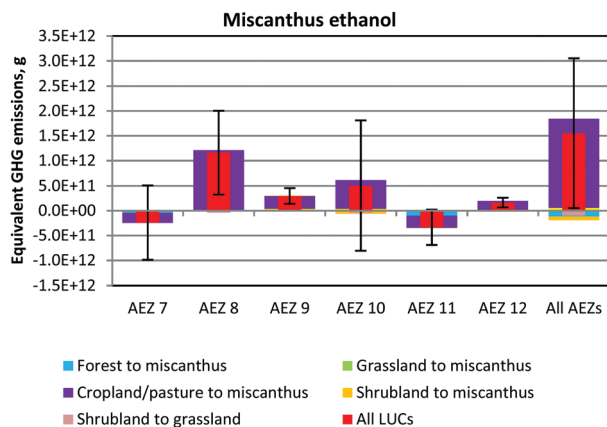**Fig. 6** Aggregated LUC-induced albedo effects at the AEZ level for switchgrass ethanol production.

Fig. 7 Aggregated LUC-induced albedo effects at the AEZ level for miscanthus ethanol production.

Fig. 8 Total LUC-induced albedo effects, in g CO_2e per MJ, of corn, switchgrass, and miscanthus ethanol in the U.S.

from cropland/pasture land to switchgrass fields reflects the net albedo effect of converting 50% of the cropland/pasture land represented by corn/soybean fields or corn/winter wheat fields to 50% of the switchgrass fields represented by grassland. Again, large variations in the albedo effect are present in AEZs 7, 8, 10, and 11, resulting in a large variation in the total albedo effect of switchgrass ethanol, which varies from 1.79 to 11.8 Tg CO_2e.

For miscanthus ethanol, the average albedo effect varies from a cooling effect in AEZs 7 and 11 to a warming effect in AEZs 8, 9, 10, and 12 (Fig. 7). A conversion from cropland/pasture land to miscanthus fields is the dominant cause of either the cooling or warming effect in each AEZ. Combining all AEZs results in a total warming effect of 1.5 Tg CO_2e for miscanthus ethanol, dominated by the warming effect from a shift of cropland/pasture land to miscanthus fields, which more than offsets a cooling effect for conversion from forest to miscanthus fields in AEZ 11. Again, large variations in the albedo effect are present in all AEZs, resulting in a large variation in the total albedo effect of miscanthus ethanol, which varies from 0.049 Tg to 3.0 Tg CO_2e.

Albedo effects, in g CO_2e per MJ, of ethanol from corn, switchgrass, and miscanthus

We quantified the albedo effects, in g CO_2 per MJ of ethanol from corn, miscanthus, and switchgrass. For corn ethanol, we aggregated the albedo effects associated with LUCs at the AEZ level on the basis of AEZ-specific average corn yield[37] (Table S19, ESI†) and the aggregated LUC-induced albedo effects at the AEZ level. For switchgrass and miscanthus ethanol, we aggregated the LUC-specific albedo effects at the AEZ level on the basis of AEZ-specific LUC acreage (Tables 2 and 3) and LUC-specific albedo effects.

The results of the albedo effects for corn, miscanthus, and switchgrass ethanol in g CO_2e per MJ of ethanol are shown in Fig. 8. With conversion from cropland/pasture land, grassland, forest, and shrubland to cornfields, corn ethanol has a net cooling albedo effect of −1.8 g CO_2e per MJ. When the spatial variation of albedo effects was considered, the LUC-induced albedo effect could range from a warming effect of 2.0 g CO_2e per MJ to a cooling effect of −5.7 g CO_2e per MJ for corn ethanol.
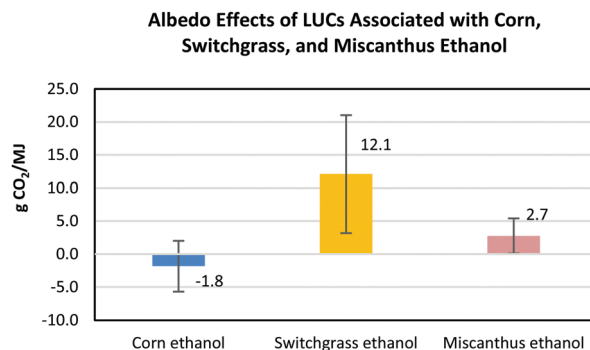
A significant warming albedo effect of 12.1 g CO_2e per MJ, on average, is found for switchgrass ethanol, as compared to life-cycle GHG emissions of about 17.3 g CO_2e per MJ for switchgrass ethanol without albedo effects.[59] The warming effect can vary from 3.2 to 21.0 g CO_2e per MJ, mostly because of the spatial variation in the albedo effect of conversion from cropland/pasture land to switchgrass fields in various AEZs. The albedo warming effect more than offsets a GHG emission reduction of −3.5 g CO_2e per MJ from increased SOC associated with the same LUCs for switchgrass ethanol production.[37]

Miscanthus ethanol has a relatively small warming albedo effect of about 2.7 g CO_2e per MJ, on average, as compared to life-cycle GHG emissions of about −6.8 g CO_2e per MJ.[59] The warming effect can vary from 0.1 to 5.4 g CO_2e per MJ, mostly because of the spatial variation in the albedo effect of conversion from cropland/pasture land to miscanthus fields in various AEZs. The albedo warming effect is relatively small, compared to a GHG emission reduction of −20.1 g CO_2e per MJ from the increased SOC associated with the same LUCs for miscanthus ethanol production.[37]

The smaller total warming albedo effect for miscanthus ethanol as compared to switchgrass ethanol is caused by two factors: (1) a smaller amount of conversion from cropland/pasture land to miscanthus fields vs. conversion to switchgrass fields (the major land conversion associated with both biofuel feedstocks) (Fig. S12, ESI†), primarily caused by the considerably higher biomass yield for miscanthus than for switchgrass;[35] and (2) the weaker warming albedo effect of this land conversion for miscanthus compared to that for switchgrass in all AEZs, except in AEZ 10 (Fig. S13, ESI†). As a result, the aggregated total albedo effects of the two biofuels differ (Fig. S14, ESI†), translating to a difference in the total albedo effect in g CO_2e per MJ, given the same volumetric amount of ethanol production from the two feedstocks.

Integration of LUC-induced albedo effects with life-cycle biogeochemical GHG emissions

We considered the impact of LUC-induced albedo effects for ethanol from corn, switchgrass, and miscanthus by integrating such effects, in g CO_2e per MJ of biofuel, with the respective life-cycle biogeochemical GHG emissions in the GREET® model as

This journal is © The Royal Society of Chemistry 2016

Energy Environ. Sci., 2016, 9, 2855–2867 | 2863

documented in our previous studies,[59] as shown in Fig. 9. With the LUC-induced albedo effect included, ethanol from corn, switchgrass, and miscanthus has life-cycle GHG emissions of 56, 29, and -4 g MJ^{-1}, respectively. These results translate to a GHG emission reduction of about 39%, 68%, and 104%, respectively, relative to petroleum-derived gasoline, which has a GHG emission intensity of 92 g CO_2e per MJ.[60] The LUC-induced albedo effect is small for corn and miscanthus ethanol, but is significant for switchgrass ethanol, reducing its GHG emission reduction relative to petroleum gasoline from about 81% without the albedo effects to 68% with the effects. These findings show that the albedo effect is biofuel feedstock-specific and can be significant for some biofuels. These results may be helpful for regulatory agencies like the U.S. EPA and California Air Resources Board to better assess the magnitude and the major drivers of this biogeophysical effect for production of major biofuels in the U.S.

In this study, we considered multiple LUC types associated with biofuel production at the AEZ level to evaluate the aggregated albedo effects of ethanol from corn, switchgrass, and miscanthus. We found that distinctive albedo effects associated with different LUC scenarios, even in the same AEZs, contributed to the difference in aggregated albedo effects for ethanol from corn, switchgrass, and miscanthus. For example, in AEZs 9–12, conversion from cropland/pasture land to cornfields, the major land cover conversion type for corn ethanol production, could lead to cooling albedo effects, whereas conversion from this land cover to switchgrass would lead to warming albedo effects. Besides, the magnitudes of the various land cover conversions varied for the three feedstocks. For example, conversions from shrubland and forest to cornfields are two major LUC types besides conversion from cropland/pasture land to cornfields in AEZs 7, 10, 11, and 12, where the cropland/pasture conversion is the dominant LUC type for switchgrass and miscanthus. Therefore, variation in the types and magnitudes of different LUC scenarios that have distinct albedo effects results in significant

differences in the overall albedo effects for ethanol from corn, switchgrass, and miscanthus.

Albedo effects are region-specific even for the same LUC scenarios. This finding was captured by the remarkable temporal and spatial variations in albedo and its radiative forcing from a large number of clean pixels that represent different locations of biomass production. This finding agrees with previous work.[31] Increasing the geographical coverage of modelling biomass production systems is a key factor to better understanding the magnitude—and variability—of the albedo effect stemming from LUCs associated with biofuel production. However, it is noted that the land classification in the CDL data could be of low accuracy in some areas.[61] Consideration of the uncertainty and biases of the CDL data[62] is worth further effort and may add to the accuracy of our analysis.

The GTAP-simulated LUC results we applied in this study did not quantify variability and uncertainty in biofuel LUC modeling. The variations in LUC-induced albedo effects that we quantified for ethanol from corn, switchgrass, and miscanthus only reflected the variability in albedo dynamics from over one million location-specific sites, and did not represent any of the potential variability of LUC *per se*, which has yet to be understood quantitatively. It is worth noting that aggregated LUC-induced albedo effects for corn ethanol, as shown in Fig. 5, were less uncertain than those for switchgrass and miscanthus, as shown in Fig. 6 and 7, mainly because additional, less certain assumptions, *e.g.* biomass yields, yield elasticities, and price elasticities, were made in the GTAP LUC simulations for the latter two than for corn. Given the fundamental impacts of the types and scales of LUC results due to biofuel production on the resultant albedo effects, further investigation is warranted for improved understanding of the variability and uncertainty of LUC-induced albedo effects.

It is noted that the GTAP LUC results that we adopted in this study are just one set of the estimates of what could happen with LUC driven by expanded biomass production for biofuel production. For corn, alternative land transitions could be crop shifting. Fig. 10 shows the changes in radiative forcings due to albedo changes for a land transition from cropland, which is represented by soybean fields in AEZs 8–12 and winter wheat fields in AEZ 7, to cornfields, and for a land transition from cropland/pasture land to cornfields. A very similar albedo effect would be expected if winter wheat fields, instead of cropland/pasture land, were converted to cornfields in AEZ 7, and a small reduction in net radiative forcing would be expected in other AEZs if soybean fields, instead of cropland/pasture land, were converted to cornfields there. Other situations being equal, a slightly reinforced cooling albedo effect would be expected for corn ethanol if cropland, instead of cropland/pasture land, were converted to cornfields for corn ethanol production. For energy grasses like switchgrass and miscanthus, an alternative land transition could be conversion from pasture, resulting in very little albedo change and albedo climate effect.

We considered only U.S. domestic LUC-induced albedo effects in this study, but did not consider any international LUC-induced albedo effects. International LUCs comprising
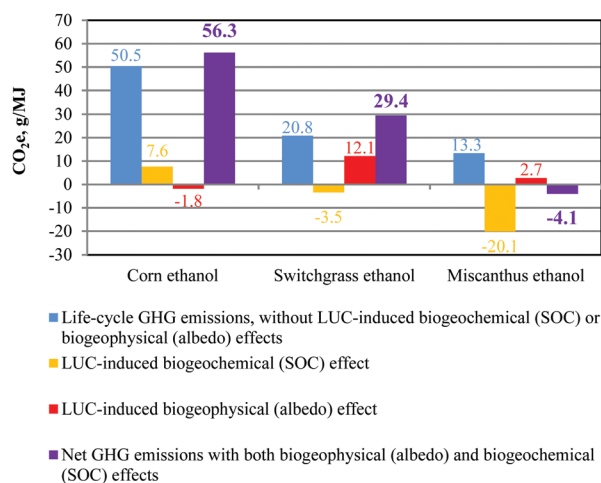
Fig. 9 Integration of LUC-induced albedo effects with life-cycle GHG emissions, including LUC-induced SOC changes, for corn, switchgrass, and miscanthus ethanol.
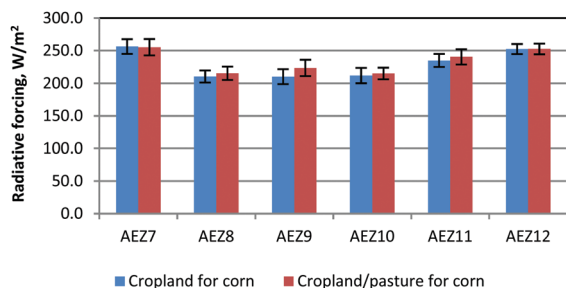
2864 | *Energy Environ. Sci.,* 2016, **9**, 2855–2867

This journal is © The Royal Society of Chemistry 2016

Fig. 10 Comparison of net radiative forcings in various AEZs, in W m^{-2}, for land transitions from cropland to cornfields, in comparison to those from cropland/pasture land to cornfields.

conversions of forest land and cropland/pasture land to land growing corn, switchgrass, and miscanthus may cause relatively smaller albedo effects than do the domestic LUCs, while international conversion from grassland to these biomass feedstocks may cause relatively more significant albedo effects than do the domestic LUCs, on the basis of a comparison of the magnitudes of domestic and international LUCs from GTAP simulations for corn, switchgrass, and miscanthus ethanol production (Table S20, ESI†). Nevertheless, additional research efforts on quantifying international LUC-induced albedo effects are needed for better understanding of aggregate albedo effects globally.

Besides, the significant variation in LUC-induced albedo effects at the AEZ level partly stems from using potentially different site-specific locations of relevant land cover types associated with a given LUC at the AEZ level, which exhibit varied site-specific albedo dynamics in response to local solar zenith angles and phenology. Improved LUC assumptions that reflect the land use history at a finer spatial resolution than AEZ, if not at the exact same locations where the LUC occur, would be needed to reduce the variability and uncertainty of quantifying LUC-induced albedo effects for these biofuels.

We were limited to using year 2014 to represent the 30 year lifetime of LUCs as a result of ethanol production. Although year 2014 represents a climatically neutral year, other factors that impact the surface albedo—including crop phenology, biomass yields, solar radiation intensities, soil water contents, ambient aerosol concentrations, and others—can change over time, and thus could result in the albedo effects over a 30 year period different from what we estimated with a single year in this analysis. Long-term dynamic analysis of albedo effects could be helpful to improve the accuracy of the albedo effect results over a period of time.

Conclusions

This study highlighted the importance of the consideration of LUC-induced albedo effects in understanding a fuller picture of the climate impacts of biofuels that traditional LCA has generally overlooked. Large-scale expansion in biofuel production aiming to reduce transportation sector GHG emissions could

have a significant LUC-induced biogeophysical impact. Using satellite observations of surface albedo dynamics over various land cover types and an advanced radiative-forcing modeling system, we quantified the albedo effects of expanded production of ethanol from corn, switchgrass, and miscanthus in the U.S. The quantified LUC-induced albedo effects were expressed in terms of CO_2e GHG emissions on the basis of the radiative forcing-based GWP metric, and directly compared to GHG emissions from processes of biofuel supply chains and from LUC-induced biogeochemical changes. While albedo effects can be substantial for certain types of land conversions associated with corn, switchgrass, and miscanthus ethanol, the total albedo effect for each of these ethanol types depends on the types and magnitudes of land conversion types and the LUC-specific albedo effect. Our study shows that the total albedo effects for corn ethanol and miscanthus ethanol are relatively small, owing partly to very different land conversion-specific albedo effects in different regions that mostly offset one another. On the other hand, switchgrass ethanol has a relatively stronger albedo effect, mostly resulting from conversion from cropland/pasture land to switchgrass fields in various regions of the U.S.

Our analysis revealed the significant spatial variations in albedo-induced climate effects for the same land conversion types across different AEZs, or for different land conversion types within the same AEZs. Thus, analysis of albedo effects for biofuel production needs to consider the types, locations, and intensities of various land conversions to improve accuracy of such analysis. In particular, our analysis demonstrated the need for finer spatial resolution of biofuel LUC in reducing the variability and uncertainty of quantifying LUC-induced biofuel albedo effects.

Glossary

AEZ	Agro-ecological zones
BSA	Black-sky albedo
CDL	Cropland data layer
CO_2e	CO_2 equivalent
CONUS	Contiguous U.S.
GHG	Greenhouse gas
GTAP	The global trade analysis project model
GWP	Global warming potential
LCA	Life-cycle analysis
LCFS	Low Carbon Fuel Standard
LUC	Land use change
MACR	The Monte Carlo aerosol, cloud and radiation model
MJ	Mega-Joule
MODIS	Moderate resolution imaging spectroradiometer
RFS	Renewable Fuel Standard
SOC	Soil organic carbon
Tg	Teragrams
TOA	Top of the atmosphere
USDA	U.S. Department of Agriculture
WSA	White-sky albedo

References

1 U.S. Environmental Protection Agency, 2016.
2 California Air Resources Board, 2015.
3 European Commission, 2009.
4 T. Searchinger, R. Heimlich, R. A. Houghton, F. Dong, A. Elobeid, J. Fabiosa, S. Tokgoz, D. Hayes and T.-H. Yu, *Science*, 2008, **319**, 1238–1240.
5 M. Claussen, V. Brovkin and A. Ganopolski, *Geophys. Res. Lett.*, 2001, **28**, 1011–1014.
6 R. A. Pielke, *Science*, 2005, **310**, 1625–1626.
7 N. de Noblet-Ducoudré, J.-P. Boisier, A. Pitman, G. B. Bonan, V. Brovkin, F. Cruz, C. Delire, V. Gayler, B. Van den Hurk and P. J. Lawrence, *et al.*, *J. Clim.*, 2012, **25**, 3261–3281.
8 G. A. Ban-Weiss, G. Bala, L. Cao, J. Pongratz and K. Caldeira, *Environ. Res. Lett.*, 2011, **6**, 34032.
9 J. J. Feddema, K. W. Oleson, G. B. Bonan, L. O. Mearns, L. E. Buja, G. A. Meehl and W. M. Washington, *Science*, 2005, **310**, 1674–1678.
10 M. M. Loranty, L. T. Berner, S. J. Goetz, Y. Jin and J. T. Randerson, *Glob. Change Biol.*, 2014, **20**, 594–606.
11 R. Alkama and A. Cescatti, *Science*, 2016, **351**, 600–604.
12 S. Luyssaert, M. Jammet, P. C. Stoy, S. Estel, J. Pongratz, E. Ceschia, G. Churkina, A. Don, K. Erb, M. Ferlicoq, B. Gielen, T. Grünwald, R. A. Houghton, K. Klumpp, A. Knohl, T. Kolb, T. Kuemmerle, T. Laurila, A. Lohila, D. Loustau, M. J. McGrath, P. Meyfroidt, E. J. Moors, K. Naudts, K. Novick, J. Otto, K. Pilegaard, C. A. Pio, S. Rambal, C. Rebmann, J. Ryder, A. E. Suyker, A. Varlagin, M. Wattenbach and A. J. Dolman, *Nat. Clim. Change*, 2014, **4**, 389–393.
13 K. Naudts, Y. Chen, M. J. McGrath, J. Ryder, A. Valade, J. Otto and S. Luyssaert, *Science*, 2016, **351**, 597–600.
14 L. R. Boysen, V. Brovkin, V. K. Arora, P. Cadule, N. de Noblet-Ducoudré, E. Kato, J. Pongratz and V. Gayler, *Earth Syst. Dyn.*, 2014, **5**, 309.
15 R. A. Betts, *Atmos. Sci. Lett.*, 2001, **2**, 39–51.
16 G. Bala, K. Caldeira, M. Wickett, T. J. Phillips, D. B. Lobell, C. Delire and A. Mirin, *Proc. Natl. Acad. Sci. U. S. A.*, 2007, **104**, 6550–6555.
17 R. A. Betts, P. D. Falloon, K. K. Goldewijk and N. Ramankutty, *Agric. For. Meteorol.*, 2007, **142**, 216–233.
18 R. M. Bright, *Environ. Sci. Technol.*, 2015, **49**, 3291–3303.
19 R. A. Betts, *Nature*, 2000, **408**, 187–190.
20 R. A. Betts, P. D. Falloon, K. K. Goldewijk and N. Ramankutty, *Agric. For. Meteorol.*, 2007, **142**, 216–233.
21 R. M. Bright, C. Antón-Fernández, R. Astrup, F. Cherubini, M. Kvalevåg and A. H. Strømman, *Glob. Change Biol.*, 2014, **20**, 607–621.
22 R. M. Bright, F. Cherubini and A. H. Strømman, *Environ. Impact Assess. Rev.*, 2012, **37**, 2–11.
23 R. M. Bright, A. H. Strømman and G. P. Peters, *Environ. Sci. Technol.*, 2011, **45**, 7570–7580.
24 M. T. Coe, T. R. Marthews, M. H. Costa, D. R. Galbraith, N. L. Greenglass, H. M. Imbuzeiro, N. M. Levine, Y. Malhi, P. R. Moorcroft and M. N. Muza, *et al.*, *Philos. Trans. R. Soc., B*, 2013, **368**, 20120155.
25 E. L. Davin and N. de Noblet-Ducoudré, *J. Clim.*, 2010, **23**, 97–112.
26 A. Lohila, K. Minkkinen, J. Laine, I. Savolainen, J.-P. Tuovinen, L. Korhonen, T. Laurila, H. Tietäväinen and A. Laaksonen, *J. Geophys. Res.: Biogeosci.*, 2010, **115**, G04011.
27 M. Georgescu, D. B. Lobell and C. B. Field, *Proc. Natl. Acad. Sci. U. S. A.*, 2011, **108**, 4307–4312.
28 P. Forster, V. Ramaswamy, P. Artaxo, T. Berntsen, R. Betts, D. W. Fahey, J. Haywood, J. Lean, D. C. Lowe, G. Myhre, J. Nganga, R. Prinn, G. Raga, M. Schulz and R. V. Dorland, Intergovernmental Panel on Climate Change Fourth Assessment Report: Climate Change 2007: Working Group I: The Physical Science Basis, Chapter 2: Changes in Atmospheric Constituents and in Radiative Forcing, 2007.
29 S. R. Loarie, D. B. Lobell, G. P. Asner, Q. Mu and C. B. Field, *Nat. Clim. Change*, 2011, **1**, 105–109.
30 K. J. Anderson-Teixeira, P. K. Snyder, T. E. Twine, S. V. Cuadra, M. H. Costa and E. H. DeLucia, *Nat. Clim. Change*, 2012, **2**, 177–181.
31 F. Caiazzo, R. Malina, M. D. Staples, P. J. Wolfe, S. H. Yim and S. R. Barrett, *Environ. Res. Lett.*, 2014, **9**, 24015.
32 Renewable Fuels Association, *World Fuel Ethanol Production*, 2016.
33 M. Wang, J. Han, J. B. Dunn, H. Cai and A. Elgowainy, *Environ. Res. Lett.*, 2012, **7**, 45905.
34 Food and Agriculture Organization of the United Nations, 2015.
35 F. Taheripour, W. Tyner and M. Wang, *GTAP Cellulosic Biofuels Analysis of Land Use Changes*, 2011.
36 J. Dunn, Z. Qin, S. Mueller, H.-Y. Kwon, M. Wander and M. Wang, *Carbon Calculator for Land Use Change from Biofuels Production (CCLUB) Manual*, 2014.
37 Z. Qin, J. B. Dunn, H. Kwon, S. Mueller and M. M. Wander, *GCB Bioenergy*, 2016, DOI: 10.1111/gcbb.12333.
38 R. A. Betts, *Nat. Clim. Change*, 2011, **1**, 99–101.
39 G. B. Bonan, *Science*, 2008, **320**, 1444–1449.
40 NASA, 2014.
41 Y. Jin, C. B. Schaaf, C. E. Woodcock, F. Gao, X. Li, A. H. Strahler, W. Lucht and S. Liang, *J. Geophys. Res.: Atmos.*, 2003, **108**, 4159.
42 Y. Jin, C. B. Schaaf, F. Gao, X. Li, A. H. Strahler, W. Lucht and S. Liang, *J. Geophys. Res.: Atmos.*, 2003, **108**, 4158.

2866 | *Energy Environ. Sci.*, 2016, **9**, 2855–2867

This journal is © The Royal Society of Chemistry 2016

43 J. Liu, C. Schaaf, A. Strahler, Z. Jiao, Y. Shuai, Q. Zhang, M. Roman, J. A. Augustine and E. G. Dutton, *J. Geophys. Res.: Atmos.*, 2009, **114**, D01106.

44 J. G. Salomon, C. B. Schaaf, A. H. Strahler, F. Gao and Y. Jin, *IEEE Trans. Geosci. Remote Sens.*, 2006, **44**, 1555–1565.

45 Z. Wang, X. Zeng, M. Barlage, R. E. Dickinson, F. Gao and C. B. Schaaf, *J. Hydrometeorol.*, 2004, **5**, 3–14.

46 F. Yang, K. Mitchell, Y.-T. Hou, Y. Dai, X. Zeng, Z. Wang and X.-Z. Liang, *J. Appl. Meteorol. Climatol.*, 2008, **47**, 2963–2982.

47 NASA, 2014.

48 U.S. Department of Agriculture, 2015.

49 F. Gao, C. B. Schaaf, A. H. Strahler, A. Roesch, W. Lucht and R. Dickinson, *J. Geophys. Res.: Atmos.*, 2005, **110**, D01104.

50 United States Department of Agriculture, *Quick Stats*, 2016.

51 Argonne National Laboratory, 2015.

52 F. Cherubini, R. M. Bright and A. H. Strømman, *Environ. Res. Lett.*, 2012, 7, 45902.

53 I. A. Podgorny and V. Ramanathan, *J. Geophys. Res.: Atmos.*, 2001, **106**, 24097–24105.

54 V. Ramanathan, P. J. Crutzen, J. Lelieveld, A. P. Mitra, D. Althausen, J. Anderson, M. O. Andreae, W. Cantrell, G. R. Cass, C. E. Chung, A. D. Clarke, J. A. Coakley, W. D. Collins, W. C. Conant, F. Dulac, J. Heintzenberg, A. J. Heymsfield, B. Holben, S. Howell, J. Hudson, A. Jayaraman, J. T. Kiehl, T. N. Krishnamurti, D. Lubin, G. McFarquhar, T. Novakov, J. A. Ogren, I. A. Podgorny, K. Prather, K. Priestley, J. M. Prospero, P. K. Quinn, K. Rajeev, P. Rasch, S. Rupert, R. Sadourny, S. K. Satheesh, G. E. Shaw, P. Sheridan and F. P. J. Valero, *J. Geophys. Res.: Atmos.*, 2001, **106**, 28371–28398.

55 R. Pincus, H. W. Barker and J.-J. Morcrette, *J. Geophys. Res.: Atmos.*, 2003, **108**, 4376.

56 H. W. Barker, G. L. Stephens, P. T. Partain, J. W. Bergman, B. Bonnel, K. Campana, E. E. Clothiaux, S. Clough, S. Cusack, J. Delamere, J. Edwards, K. F. Evans, Y. Fouquart, S. Freidenreich, V. Galin, Y. Hou, S. Kato, J. Li, E. Mlawer, J.-J. Morcrette, W. O'Hirok, P. Räisänen, V. Ramaswamy, B. Ritter, E. Rozanov, M. Schlesinger, K. Shibata, P. Sporyshev, Z. Sun, M. Wendisch, N. Wood and F. Yang, *J. Clim.*, 2003, **16**, 2676–2699.

57 Intergovernmental Panel on Climate Change, 2014.

58 R. G. Pearson, S. J. Phillips, M. M. Loranty, P. S. A. Beck, T. Damoulas, S. J. Knight and S. J. Goetz, *Nat. Clim. Change*, 2013, **3**, 673–677.

59 Argonne National Laboratory, 2016.

60 H. Cai, A. R. Brandt, S. Yeh, J. G. Englander, J. Han, A. Elgowainty and M. Wang, *Environ. Sci. Technol.*, 2015, **49**, 8219–8227.

61 K. D. Reitsma, D. E. Clay, S. A. Clay, B. H. Dunn and C. Reese, *Agron. J.*, 2016, **108**, 266.

62 T. J. Lark, J. M. Salmon and H. K. Gibbs, *Environ. Res. Lett.*, 2015, **10**, 44003.

This journal is © The Royal Society of Chemistry 2016

Energy Environ. Sci., 2016, **9**, 2855–2867 | 2867